PCCP

PAPER

View Article Online
View Journal | View Issue

Published on 29 novembr 2013. Downloaded by University of Chicago on 2020.04.13. 2:21:20.

Cite this: *Phys. Chem. Chem. Phys.*, 2014, **16**, 2297

The influence of transition metal oxides on the kinetics of Li_2O_2 oxidation in Li–O_2 batteries: high activity of chromium oxides†

Koffi P. C. Yao,[a] Yi-Chun Lu,‡[b] Chibueze V. Amanchukwu,[c] David G. Kwabi,[a] Marcel Risch,[a] Jigang Zhou,[d] Alexis Grimaud,[a] Paula T. Hammond,[c] Fanny Bardé[e] and Yang Shao-Horn*[ab]

Received 14th October 2013,
Accepted 28th November 2013

DOI: 10.1039/c3cp53330a

www.rsc.org/pccp

Reducing the energy loss associated with Li_2O_2 electrochemical oxidation is paramount to the development of efficient rechargeable lithium–oxygen (Li–O_2) batteries for practical use. The influence of a series of perovskites with different e_g filling on the kinetics of Li_2O_2 oxidation was examined using Li_2O_2-prefilled electrodes. While $LaCrO_3$ is inactive for oxygen evolution upon water oxidation in alkaline solution, it was found to provide the highest specific current towards Li_2O_2 oxidation among all the perovskites examined. Further exploration of Cr-based catalysts showed that Cr nanoparticles (Cr NP) with an average particle size of 40 nm, having oxidized surfaces, had comparable surface area activities to $LaCrO_3$ but much greater mass activities. Unlike Pt/C and Ru/C that promote electrolyte oxidation in addition to Li_2O_2 oxidation, no evidence of enhanced electrolyte oxidation was found for Cr NP relative to Vulcan carbon. X-ray absorption spectroscopy at the O K and Cr L edge revealed a redox process of $Cr^{3+} \leftrightarrow Cr^{6+}$ on the surface of Cr NP upon Li_2O_2 oxidation, which might be responsible for the enhanced oxidation kinetics of Li_2O_2 and the reduced charging voltages of Li–O_2 batteries.

Introduction

Nonaqueous lithium–oxygen (Li–O_2) batteries, which form lithium peroxide (Li_2O_2) on discharge, have the potential to deliver gravimetric energy three to five times greater than that of current state of the art Li-ion batteries.[1–3] Unfortunately, charging of Li–O_2 batteries requires large overpotentials, even with ether-based electrolytes, which are relatively stable against reaction intermediates upon oxygen reduction such as superoxide,[4–8] notwithstanding the minor presence of electrolyte decomposition products during the first cycle.[7,9,10] The electro-oxidation of thin Li_2O_2 deposits ($< \sim 1$ nm)[11–15] or the early stage of charging[16] can proceed with overpotentials smaller than $\sim$500 mV. In contrast, large overpotentials greater than $\sim$1000 mV are noted typically in the electro-oxidation of Li_2O_2 deposits with thicknesses greater than $\sim$5 nm and at high rates ($\sim$1 μA cm_{true}^{-2}).[12–14,16–19] To realize the gravimetric energy advantage of Li–O_2 batteries over Li-ion batteries, it is necessary to enable facile formation and oxidation kinetics of Li_2O_2 deposits (with thicknesses greater than a few nanometers) within the electrode pore volume during discharge and charge.

Although the physical origin of the large overpotentials associated with Li_2O_2 oxidation is not well understood, the following factors have been shown to influence the charging voltage from previous studies. First, electrolyte solvents such as dimethylformamide[20] and dimethylsulfoxide[21] provide lower charging voltages ($\sim$3.6 V_{Li} at 0.1 μA cm_{carbon}^{-2} or 70 mA g_{carbon}^{-1}) compared to ether-based solvents using carbon electrodes. Unfortunately these solvents are not stable against lithium metal.[21,22] Second, molecular catalysts have recently enabled charging of carbon cathodes in Li–O_2 cells at $\sim$3.6 V_{Li}.[23,24] Third, Harding *et al.*[25] have shown that noble metals such as Pt and Ru nanoparticles supported on carbon can promote the oxidation kinetics

[a] *Department of Mechanical Engineering, Massachusetts Institute of Technology, 77 Massachusetts Avenue, Cambridge, MA 02139, USA. E-mail: shaohorn@mit.edu*
[b] *Department of Materials Science and Engineering, Massachusetts Institute of Technology, 77 Massachusetts Avenue, Cambridge, MA 02139, USA*
[c] *Department of Chemical Engineering, Massachusetts Institute of Technology, 77 Massachusetts Avenue, Cambridge, MA 02139, USA*
[d] *Canadian Light Source Inc., University of Saskatchewan, Saskatoon, SK S7N 0X4, Canada*
[e] *Toyota Motor Europe, Research & Development 3, Advanced Technology 1, Hoge Wei 33 B, B-1930 Zaventem, Belgium*

† Electronic supplementary information (ESI) available: Perovskite synthesis details, details of background subtraction, ^{1}H NMR spectra, SEM images post charge and discharge, XRD of the Cr discharge product, summary of literature data on oxide catalysis, SEM calculated surface areas of perovskite catalysts, and background current of Cr-catalyzed electrodes. See DOI: 10.1039/c3cp53330a

‡ Present address: Department of Mechanical and Automation Engineering, The Chinese University of Hong Kong, Hong Kong, P. R. China.

Published on 29 novembr 2013. Downloaded by University of Chicago on 2020.04.13. 2:21:20.

of Li_2O_2 particles (~345 nm) and achieve oxidation currents hundredfold higher than that of carbon-only electrodes using 0.1 M $LiClO_4$ in 1,2-dimethoxyethane (DME) as the electrolyte, allowing Li_2O_2 oxidation at ~3.5 V_{Li}. Unfortunately, the greater kinetics for Li_2O_2 electrochemical oxidation with these noble metal catalysts are accompanied by enhanced electrolyte oxidation. Fourth, non-noble metal oxides have been used to lower the charging voltages of Li–O_2 cells[17,18,26] or Li_2O_2-filled[27,28] electrodes, as summarized in Table S1 (ESI†), where only studies with ether-based electrolytes are included. For example, $Na_{0.44}MnO_2$ (ref. 18, 70 mA g_{carbon}^{-1}, carbon/oxide weight ratio of 1 : 0.4), and $Pb_2[Ru_{1.7}Pb_{0.3}]O_{6.5}$ pyrochlores[17,29] (70 mA g_{carbon}^{-1}, carbon/oxide weight ratio of 1 : 1) have shown ~3.9 V_{Li} for Li_2O_2 oxidation while the layered-perovskite[28] $La_{1.7}Ca_{0.3}Ni_{0.75}Cu_{0.25}O_4$ provides charging at ~3.6 V_{Li}, albeit at a lower rate of 20 mA g_{carbon}^{-1} and a carbon/oxide weight ratio of 1 : 0.3. As carbon/oxide ratios, oxide/Li_2O_2 ratios, and the surface area of oxides and Li_2O_2 in these previous studies[17,18,29] vary greatly, ambiguities exist in deducing the oxide activities for Li_2O_2 oxidation kinetics by comparing the reported charging voltages of different oxides across these studies.

In this study, we systematically measure the activities of a number of perovskites for Li_2O_2 electrochemical oxidation using Li_2O_2-preloaded electrodes. Our recent studies in alkaline media have shown that the intrinsic activities of oxygen reduction and oxygen evolution kinetics of transition metal oxides can be tuned by several orders of magnitude using e_g orbital filling of transition metal ions.[30,31] The use of e_g orbital filling as an activity descriptor led to the identification of $Ba_{0.5}Sr_{0.5}Co_{0.8}Fe_{0.2}O_{3-\delta}$ (BSCF) with the record intrinsic activity for oxygen evolution.[31] Here we examine whether such a correlation exists for the kinetics of nonaqueous Li_2O_2 electrochemical oxidation, where $LaCrO_3$, BSCF, $LaNiO_3$, $LaMnO_{3+\delta}$, and $LaFeO_3$ with e_g filling[30,31] in the range from 0 to 2 are employed. Electrodes that have fixed weight ratios of Li_2O_2/carbon and carbon/oxides are used to provide systematic comparison of oxide activities, where the particle sizes of all perovskites are comparable and Li_2O_2 particle sizes are comparable among all electrodes. We report that the Li_2O_2 oxidation kinetics are enhanced by $LaCrO_3$ and BSCF compared to Vulcan carbon (VC). Furthermore, Cr-based oxides show comparable intrinsic activities and Cr nanoparticles (Cr NP) can enable charging of Li–O_2 cells at 3.8 V_{Li} at 100 mA g_{carbon}^{-1}.

Experimental procedure

Electrode fabrication

Five perovskites including $LaCrO_3$, BSCF, $LaNiO_3$, $LaMnO_{3+\delta}$, and $LaFeO_3$ were synthesized by co-precipitation and nitrate combustion methods[30–32] (details provided in ESI†). All perovskites were sufficiently phase pure with less than 1% impurities observed by X-ray diffraction (Fig. S1, ESI†). All perovskite powder samples were ball-milled separately using a planetary ball mill (Pulverisette 6, Fritsch Inc., zirconia crucible sealed under argon) at 500 rpm to yield particle sizes of 200 to 1000 nm (1–4 m^2 $g_{perovskite}^{-1}$ in Table S2 in ESI†). Li_2O_2 (Alfa Aesar, Purity >90%) powder was also ball-milled under the same conditions to yield an average particle size of ~345 nm. Lithium-exchanged Nafion® (Ion Power USA, LITHion™, 7.2 wt%) was used as an electrode binder and VC (Vulcan XC72, Premetek Inc., 100 m^2 g^{-1}) served as the conductive matrix. Mass ratios of electrode components were set to oxide catalyst : VC : Li_2O_2 : Nafion® = 3 : 1 : 1 : 1 to yield a carbon loading of 0.21 ± 0.05 mg cm^{-2}, which was chosen to compensate for the low surface area of perovskites. In addition, the electrochemical activities of Cr_2O_3 (Sigma Aldrich, <100 nm, ~20 m^2 g^{-1}) and high-surface-area chromium nanoparticles (US Research Nanomaterials Inc., ~40 nm, ~24 m^2 g^{-1}) dispersed on carbon were measured, where mass ratios of electrode components were set to Cr : VC : Li_2O_2 : Nafion® = 0.66 : 1 : 1 : 1, and carbon loading to 0.51 ± 0.03 mg cm^{-2}. The expected capacity for complete oxidation of Li_2O_2 in all these electrodes was 1168 mA h g_{carbon}^{-1}. Moreover, VC electrodes with a mass ratio of VC : Li_2O_2 : Nafion® = 1 : 1 : 1 were fabricated for comparison. Lastly, electrodes containing VC, oxide, and Nafion®, but free of Li_2O_2 were fabricated to determine the background oxidation current of electrodes upon charging, which might result from parasitic reactions such as electrolyte oxidation. Prior to electrode fabrication, VC and catalyst powders were dried at 100 °C in a Buchi® B-585 vacuum oven for 24 hours. Transfer to an argon-filled glovebox (MBraun®, H_2O < 0.1 ppm and O_2 < 1%) from the Buchi® glass oven occurred with samples still under vacuum. All fabrication tools were dried at 70 °C overnight prior to use. VC, perovskite oxide, Li_2O_2, and Nafion® were homogenized in anhydrous 2-propanol (IPA) by probe pulse sonication at 40 W for one hour. Electrodes were fabricated by liquid film coating on an aluminum foil using a #50 Mayer rod.

O_2 electrodes for Li–O_2 cells were prepared by coating ultrasonicated inks composed of VC, Nafion®, with and without Cr NP and IPA onto the separator (Celgard C480) inside the argon-filled glovebox. The mass ratio in the oxygen electrodes was set to Cr : VC : Nafion® = 2 : 1 : 0.5, which is compared to carbon electrodes of VC : Nafion® = 1 : 0.5.

Half-inch-diameter electrodes were punched after complete evaporation of the IPA and dried at 70 °C in the Buchi® vacuum oven for at least 12 hours prior to use. Dried electrodes were directly transferred to the glove box without exposure to air. Synthesis and handling of electrodes were entirely performed in the argon-filled MBraun® glovebox. No instance of exposure to atmospheric moisture occurred from powder drying to electrode fabrication to cell construction.

Carbon-free electrodes of Cr : Li_2O_2 = 0.66 : 1 were prepared for soft X-ray absorption (XAS) studies. The absence of carbon allowed unambiguous investigation of the effect of Cr on the Li_2O_2 oxidation. Cr NP and Li_2O_2 were mixed in the desired mass ratio (no added Nafion® binder) and homogenized by sonication in IPA. After homogenization, the slurry was drop casted onto one-centimeter diameter gold disks at a target loading of ~1 mg_{Cr} cm^{-2}. After evaporation of the IPA, two gold disks were stacked, sandwiching the Cr : Li_2O_2 deposit. The sandwich structure is sealed in a heat-seal bag before

 This journal is © the Owner Societies 2014

Published on 29 novembr 2013. Downloaded by University of Chicago on 2020.04.13. 2:21:20.

removing from the glovebox to be pressed at ~600 MPa under a hydraulic press. The gold-supported electrodes prepared entirely under inert argon are dried similarly to the Nafion® bonded electrodes before electrochemical and XAS studies.

Cell making and electrochemical testing

The Li_2O_2-preloaded electrodes were charged potentiostatically in two-electrode cells (TJ-AK; Tomcell Japan Inc.) as described elsewhere.[25] The cells consisted of a stack of metallic lithium anode (Chemetall, Germany, 18 mm diameter), two Celgard 2500 separators (Celgard, USA, 21 mm diameter) and the electrode of study. Separators were wetted with ~125 μL of the electrolyte (0.1 M $LiClO_4$ in DME, Novolyte USA, H_2O <20 ppm). The cells were assembled in the argon-filled glovebox. The activity of electrochemical oxidation of Li_2O_2 with each catalyst was defined as the net oxidation current after subtracting the background oxidation current associated with charging Li_2O_2-free electrodes (details of subtraction provided in ESI,† Fig. S2), which was then normalized to the mass of carbon or the catalyst surface area.

Li–O_2 cells consisted of a lithium metal anode (Chemetall, Germany, 15 mm in diameter) and a Nafion®-bonded VC-based O_2 electrode (12.7 mm in diameter). All Li–O_2 single cells were assembled with 0.1 M $LiClO_4$ in DME electrolyte in the glovebox. The assembling procedures of Li–O_2 cells were reported previously.[33] The assembled cells were purged with oxygen for ten minutes before testing. These Li–O_2 cells were tested galvanostatically using a Solartron 1470 (Solartron Analytical, UK).

Electrode characterization

X-ray diffraction (XRD) patterns of the Li_2O_2-preloaded electrodes were collected before and after charging using a PANanalytical X'Pert Pro™ diffractometer in Bragg–Brentano geometry. XRD was also used to characterize the discharge product(s) of Li–O_2 cells. The oxidation state of surface chromium in $LaCrO_3$, Cr_2O_3 and Cr NP was probed using X-ray photoelectron spectroscopy (XPS, Physical Electronics Versaprobe II). Spectra collected in the Cr 2p binding energy-range (570 to 600 eV) were analyzed using the CasaXPS software. The electrode morphologies of Li_2O_2-preloaded electrodes before and after charging, and of the O_2 electrode with Cr NP before and after discharge were investigated using a JEOL 6320F high-resolution scanning electron microscope (SEM) at an acceleration voltage of 5 kV.

XAS studies of carbon-free chromium electrodes were performed at the SGM beamline of the Canadian Light Source.[34] O K and Cr $L_{2,3}$ edge spectra were collected in total electron yield (TEY) mode under vacuum below 10^{-7} torr at room temperature. The energy axis was calibrated using the simultaneously measured L_2-edge of metallic Cr. The O K and Cr L-edge absorptions were extracted by fitting a first order polynomial in the pre-edge region, extrapolating over the entire range of the spectrum and subtracting this background from the spectrum. The edge height of the XAS was normalized to unity by division of a constant obtained by fitting the postedge spectrum. Spectra of the as-purchased Cr NP, and the gold-supported Cr : Li_2O_2 electrodes in the pristine, partially charged, and fully charged states were of interest.

Results and discussion

Influence of perovskites on the kinetics of Li_2O_2 electrochemical oxidation

The kinetics of Li_2O_2 oxidation by $LaNiO_3$, $LaMnO_{3+\delta}$, and $LaFeO_3$ were found to exhibit similar activities to VC. The net oxidation currents obtained from $LaNiO_3$, $LaMnO_{3+\delta}$, $LaFeO_3$, and VC at 4.0 V_{Li}, which were normalized to carbon weight in the Li_2O_2-preloaded electrodes, are shown in Fig. 1a, where the current densities first rose and then decayed with time. It should be mentioned that VC had oxidation currents of Li_2O_2 oxidation in agreement with previous work.[25] In contrast, electrodes with $LaCrO_3$ and BSCF had higher activities (Fig. 1b), where mass-specific net oxidation currents of $LaCrO_3$ and BSCF were greater than that of VC by one order of magnitude. All electrodes were found to deliver ~90% of expected capacity based on the

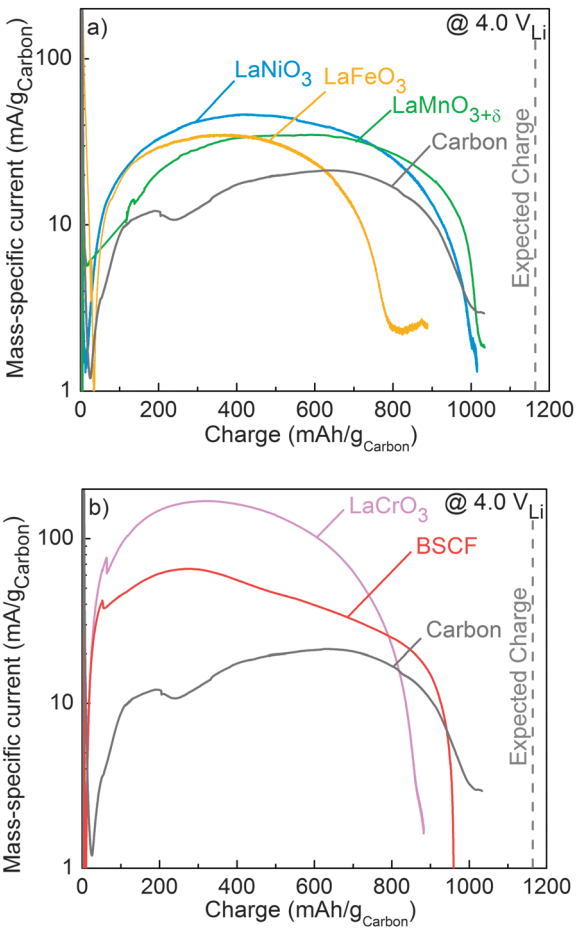

Fig. 1 Net current of Li_2O_2 oxidation normalized to carbon mass of Li_2O_2-preloaded electrodes obtained from potentiostatic holding of 4.0 V_{Li}. The Li_2O_2-preloaded electrodes have a mass ratio of perovskite : VC : Li_2O_2 = 3 : 1 : 1 with a carbon loading of 0.21 ± 0.05 mg cm^{-2}. (a) Mass-specific activities of electrodes with (a) $LaFeO_3$, $LaNiO_3$, $LaMnO_{3+\delta}$, and (b) $LaCrO_3$ and BSCF compared to VC electrodes.

Published on 29 novembr 2013. Downloaded by University of Chicago on 2020.04.13. 2:21:20.

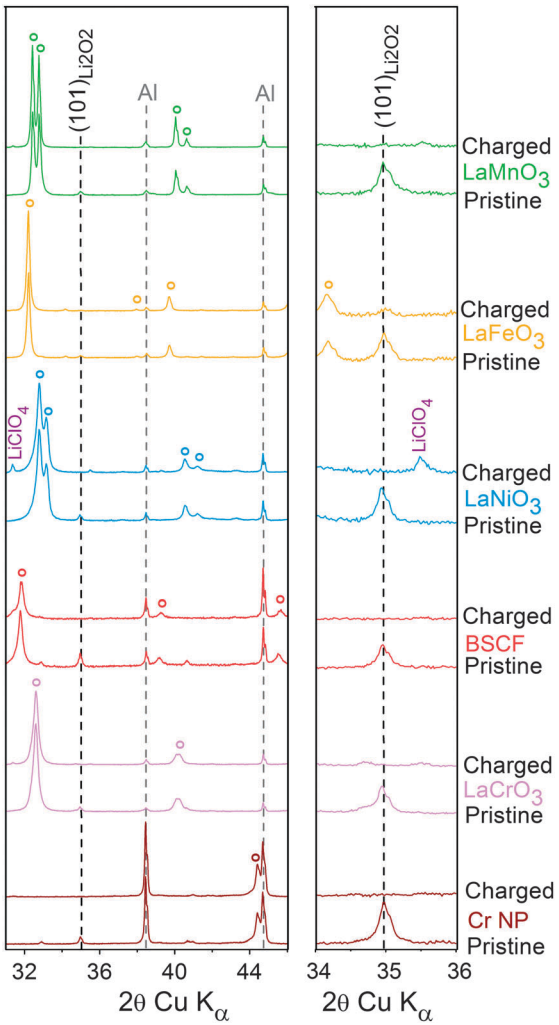

Fig. 2 XRD patterns of Li_2O_2-preloaded electrodes before and after potentiostatic charging at 4 V_{Li} (Fig. 1). (Left): XRD scan in 31 to 46 degrees in 2θ showing the presence of the reflections from the oxide catalysts (open circles) and Li_2O_2. (Right): XRD scans magnified in the region with the strongest Li_2O_2 peak at ~34.97° of Li_2O_2 from the (101) plane which was found to disappear after charging, indicating effective oxidation of the preloaded Li_2O_2.

amount of Li_2O_2 loaded in the electrode (1168 mA h g_{carbon}^{-1}), which suggests that Li_2O_2 was removed largely from these electrodes upon potentiostatic charging at 4.0 V_{Li}. This hypothesis is further supported by the following: (i) XRD of the Li_2O_2 preloaded electrode before and after complete charging showed the disappearance of Li_2O_2 reflections, as shown in Fig. 2; and (ii) removal of Li_2O_2 particles in the SEM images (Fig. S3, ESI†) after potentiostatic charging.

The activities of $LaCrO_3$ and BSCF for Li_2O_2 oxidation were further examined as a function of applied potentials from 3.8 to 4.1 V_{Li}, as shown in Fig. 3a and Fig. S4 (ESI†). Although the net oxidation currents were found to decrease with decreasing charging potential, $LaCrO_3$ remained active for Li_2O_2 oxidation at voltages as low as 3.8 V_{Li}. The average currents of Li_2O_2 oxidation of $LaCrO_3$ and BSCF during the first 20% capacity upon potentiostatic charging are shown as a function of

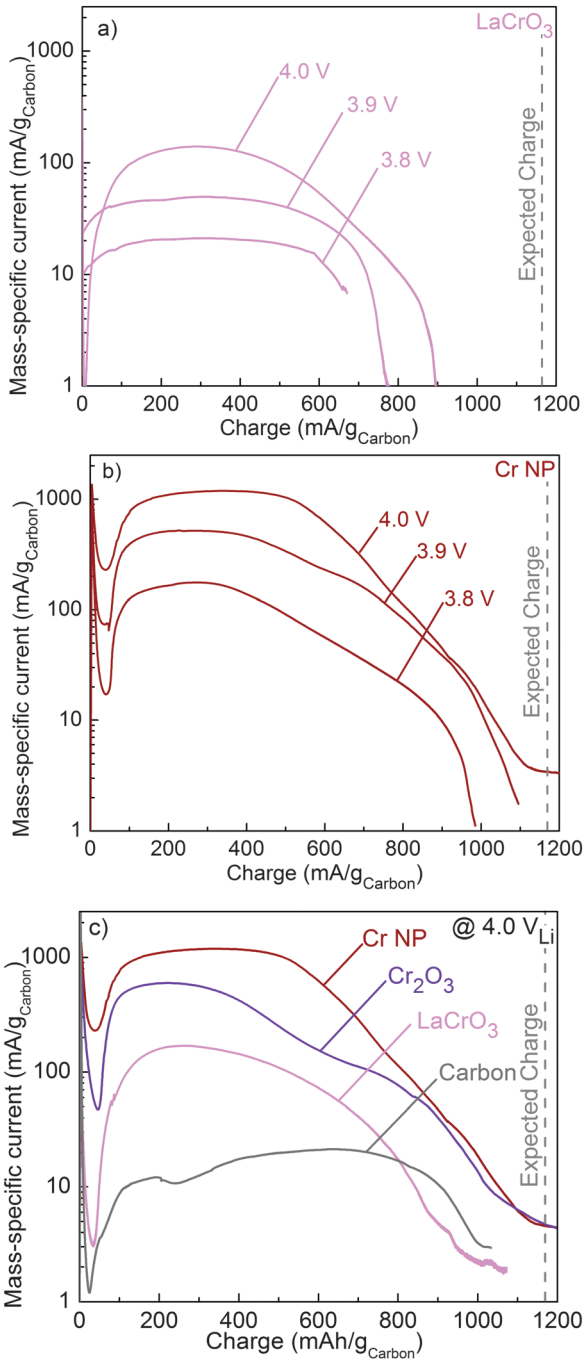

Fig. 3 Net currents normalized to carbon mass from potentiostatic charging of (a) $LaCrO_3$: VC : Li_2O_2 (3 : 1 : 1 mass ratio), (b) Cr-nanoparticles : VC : Li_2O_2 (0.66 : 1 : 1 mass ratio). (c) Mass-specific activity of electrodes with chromium oxides and Cr NPs (Cr-Oxide : VC : Li_2O_2 = 3 : 1 : 1 and Cr nanoparticles : VC : Li_2O_2 = 0.66 : 1 : 1 mass ratio) charged at 4.0 V_{Li}.

applied potential in Fig. 4 (see Fig. S5 in ESI† for details of averaging). Both mass-specific and oxide-surface-area-specific net oxidation currents of $LaCrO_3$ and BSCF for Li_2O_2 oxidation were considerably higher than VC and Au/C reported previously,[25] as shown in Fig. 4a and b, respectively. $LaCrO_3$ was found to provide the highest oxidation currents for Li_2O_2 oxidation among all the five perovskites studied, having

 This journal is © the Owner Societies 2014

Published on 29 novembr 2013. Downloaded by University of Chicago on 2020.04.13. 2:21:20.

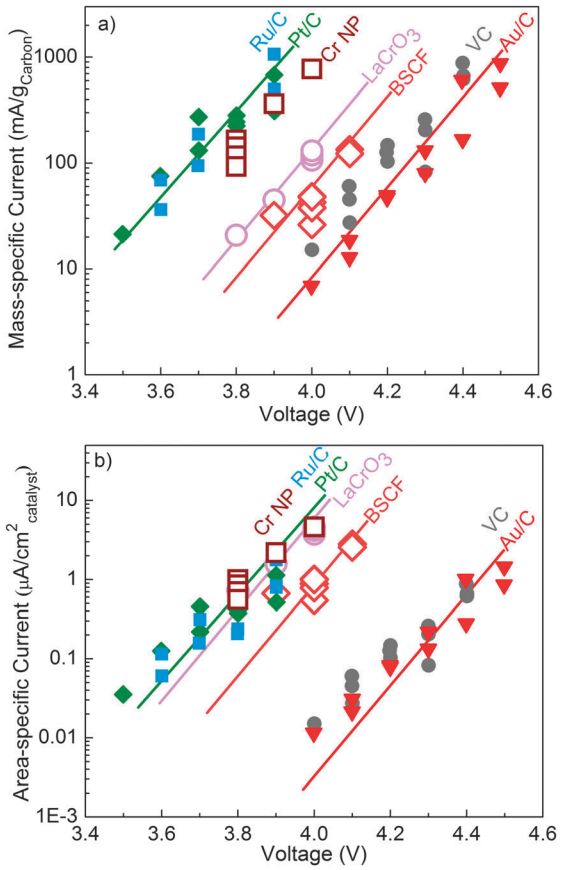

Fig. 4 (a): Net mass-specific activity *vs.* potential for $LaCrO_3$, BSCF and Cr NPs compared to Au/C, Pt/C, Ru/C and VC only electrodes reported previously[25] (Cr, Pt, Ru, Au : VC : Li_2O_2 = 0.66 : 1 : 1; perovskite : VC : Li_2O_2 = 3 : 1 : 1, mass ratios) (b): Net surface-area specific activity *vs.* potential. Specific activity of chromium nanoparticles was in good agreement with that of $LaCrO_3$.

~4 times higher area-specific oxidation currents than BSCF. Although net mass-specific oxidation currents of $LaCrO_3$ and BSCF for Li_2O_2 oxidation were lower than those of Pt/C and Ru/C reported previously,[25] the surface-area-specific currents of $LaCrO_3$ rival those of Pt/C and Ru/C,[25] and shown in Fig. 4b. The low mass-specific activity of $LaCrO_3$ compared to that of Pt/C and Ru/C (Fig. 4a) resulted from much larger particle sizes of perovskites (0.5–1 μm for $LaCrO_3$ *vs.* 3–4 nm for Pt nanoparticles and Ru nanoparticles) and thus lower specific surface area (~1 m^2 g^{-1} for $LaCrO_3$ *vs.* ~100 m^2 g^{-1} for Pt and Ru nanoparticles supported on VC).

The apparent Tafel slopes of Li_2O_2 electrochemical oxidation with $LaCrO_3$ and BSCF were ~250 mV per decade, which are comparable to those of Li_2O_2-preloaded electrodes with VC, Au/C, Pt/C and Ru/C.[25] The physical origin of such large Tafel slopes for Li_2O_2 oxidation is not well understood. It may result from coupled chemical and electrochemical reaction steps associated with Li_2O_2 electrochemical oxidation. It should be noted that Tafel slopes of Li_2O_2 electrochemical oxidation are considerably smaller than the 300 to 340 mV per decade found for charging of Li–O_2 cells.[13,16] Possible "poisoning" effects associated with parasitic reaction products formed in Li–O_2 cells such as Li_2CO_3 on the Li_2O_2 surface can be responsible for the greater Tafel slope measured for the charging of electrochemically formed Li_2O_2 compared to Li_2O_2-preloaded electrodes.

No clear trend in the activities of these perovskites against Li_2O_2 oxidation ($LaCrO_3$ ≫ BSCF > $LaNiO_3$ ≈ $LaMnO_{3+\delta}$ ≈ $LaFeO_3$) *versus* the e_g filling of the perovskites[30,31] was found. The area-specific activities of the five perovskites were correlated to their e_g filling, as shown in Fig. S6 (ESI†). This observation is in contrast to the clear volcano trend for oxygen evolution kinetics during water oxidation in 0.1 M KOH reported by Suntivich *et al.*[31] (BSCF ≫ $LaNiO_3$ ≈ $LaFeO_3$ ≫ $LaMnO_{3+\delta}$ ≈ $LaCrO_3$). $LaCrO_3$, the least active perovskite for oxygen evolution in alkaline solution was found to be the most active for Li_2O_2 oxidation. This finding is in agreement with the lowered overpotential upon charging of Li–O_2 cells with Co_3O_4,[35] which also has low activity for oxygen evolution in alkaline media.[36] The striking difference in the activity trend observed suggests different reaction mechanisms for oxygen evolution from H_2O oxidation to Li_2O_2 oxidation. We propose a different mechanism relying on the reversible redox of Cr NP upon Li_2O_2 oxidation discussed further below.

Influence of Cr-based catalysts on the kinetics of Li_2O_2 oxidation

We further examined the influence of Cr_2O_3 and Cr nanoparticles on the Li_2O_2 oxidation kinetics using Li_2O_2-filled electrodes. Cr NP were found to have much higher mass-specific currents for Li_2O_2 oxidation than $LaCrO_3$ and Cr_2O_3 (Fig. 3c), where the mass-specific activity was increased by ~50 times in the presence of Cr NP relative to VC (Fig. 4a). The removal of Li_2O_2 was confirmed by XRD (Fig. 2) and SEM imaging (Fig. S7, ESI†). Cr NP matched noble metal Pt/C and Ru/C in mass-activity (Fig. 4a) and remained active for Li_2O_2 oxidation at 3.8 V_{Li} (Fig. 3b). Unlike Pt/C and Ru/C that promote electrolyte oxidation in addition to Li_2O_2 oxidation,[25] no evidence of the enhanced electrolyte oxidation was found for Cr NP relative to VC. Much lower background oxidation currents of the electrolyte were found in the presence of Cr NP as compared to Pt/C and Ru/C (Fig. S8 and S9, ESI†). This observation is in agreement with the findings of ^{1}H NMR analysis of organic salts in the charged Cr:C background electrode (without Li_2O_2) (Fig. S10, ESI†), which showed the absence of lithium formate (HCOOLi) and lithium acetate (CH_3COOLi)[6,7] typically found upon electrolyte decomposition. Although lithium formate (HCOOLi) and lithium acetate (CH_3COOLi) were detected by ^{1}H NMR in the charged Cr:C:Li_2O_2 and C:Li_2O_2 electrodes to 4.0 V_{Li} (Fig. S10, ESI†), Cr NP were found not to enhance electrolyte decomposition. This hypothesis is supported by the termination capacity of Cr:C:Li_2O_2 electrodes (Fig. 3b) being reasonably close (85–98%) to the expected preloaded Li_2O_2 capacity unlike preloaded Li_2O_2 electrodes catalyzed by Pt/C and Ru/C,[25] indicating minimal electrolyte oxidation during charging.

The surface-area-specific activity of Cr NP was shown to be comparable to that of $LaCrO_3$ (Fig. 4b). As XPS analysis revealed Cr^{3+} and Cr^{6+} as the oxidation states common to all surfaces in $LaCrO_3$, Cr_2O_3 and Cr NP (Fig. 5a), it is proposed that the mixed

Published on 29 novembr 2013. Downloaded by University of Chicago on 2020.04.13. 2:21:20.

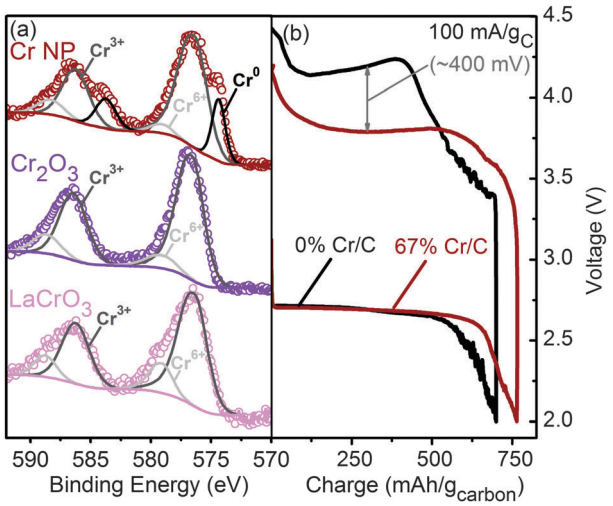

Fig. 5 XPS spectra of Cr-based catalysts, where the surfaces of Cr NP, Cr_2O_3 and $LaCrO_3$ contain both Cr^{3+} and Cr^{6+}. (b) Discharge and charge voltage profiles of Li–O_2 cells with Cr NPs (Cr NP : VC : Nafion® = 2 : 1 : 0.5) and VC (VC : Nafion® = 1 : 0.5) in the oxygen electrode tested at 100 mA g_{carbon}^{-1}.

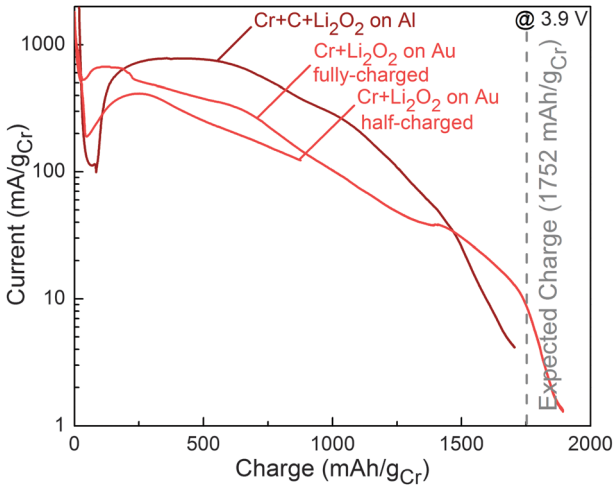

Fig. 6 Net currents normalized to Cr NP mass from potentiostatic charging of Cr NP : VC : Li_2O_2 (0.66 : 1 : 1 mass ratio) and carbon-free Cr NP : Li_2O_2 (0.66 : 1 mass ratio) pressed into an Au disk. The carbon-free electrodes were used for XAS.

valence states of Cr ions on the surfaces of Cr-containing catalysts are involved in promoting Li_2O_2 oxidation kinetics. The fast kinetics of Li_2O_2 oxidation on Cr NP mechanically mixed with VC was further confirmed in Li–O_2 cells, where the charging of crystalline ~200-nm Li_2O_2 particles (Fig. S11 and S12, ESI†) occurred at ~3.8 V_{Li} under 100 mA g_{carbon}^{-1} yielding a ~400 mV reduction on the charging overpotential compared to VC (Fig. 5b).

Proposed mechanism for enhanced Li_2O_2 oxidation kinetics with Cr

We hypothesize that the kinetics of Li_2O_2 oxidation can be influenced by the ability to promote the presence of oxygen-rich $Li_{2-x}O_2$ species, where electron transfer in the first-electron-oxidation step can be rate-limiting ($Li_2O_2 \rightarrow LiO_2 + Li^+ + e^-$), and LiO_2-like species can disproportionate chemically or get oxidized electrochemically to evolve O_2 gas.[13,37] Upon the formation of LiO_2-like surfaces ($Li_{2-x}O_2$),[13,37] further decomposition can proceed through disproportionation reactions ($2LiO_2 \rightarrow Li_2O_2 + O_2$) or through further oxidation of the LiO_2-like species. This hypothesis is relevant to but different from previous work,[35] which has suggested enhanced transport of Li_xO_2 to be responsible for greater kinetics of Li_2O_2 oxidation on Co_3O_4. We here discuss the following observations in support of this hypothesis. First, oxidation of very thin Li_2O_2 (<1 nm in thickness),[11–15] where electron transfer to the Li_2O_2 surface can be facilitated by electron tunneling,[14] occurs at low charge potentials of ~3.3 V_{Li}. Second, charging Li_2O_2 deposits (with particle sizes of 10–20 nm) at exceptionally low rates (5 mA g_{CNT}^{-1} or 0.001 μA cm_{CNT}^{-2})[16] can proceed at ~3.3 V, where electron transfer in the first-oxidation step is no longer limiting. Third, facilitating electron transfer to Li_2O_2 by molecular catalysts can lower the charge voltages to ~3.5 V.[23,24] Moreover, we use XAS data for charged electrodes to show the redox of $Cr^{3+} \leftrightarrow Cr^{6+}$ and possible formation of LiO_2 superoxide, which will be discussed below.

XAS analysis of charged preloaded Li_2O_2 electrodes with Cr NP revealed that the oxidation of Cr^{3+} to Cr^{6+} accompanied Li_2O_2 oxidation. Carbon-free, preloaded Li_2O_2 electrodes were used in these XAS experiments, which had comparable Li_2O_2 oxidation current densities normalized to the mass of Cr NP compared to electrodes with VC, as shown in Fig. 6. The XAS O K and Cr $L_{2,3}$-spectra of as-purchased Cr NP, pristine, partially charged, and fully-charged Cr:Li_2O_2 supported on Au electrodes are shown in Fig 7. Both O K and Cr $L_{2,3}$ spectra of as-purchased Cr NP resemble those of Cr_2O_3 reported in the

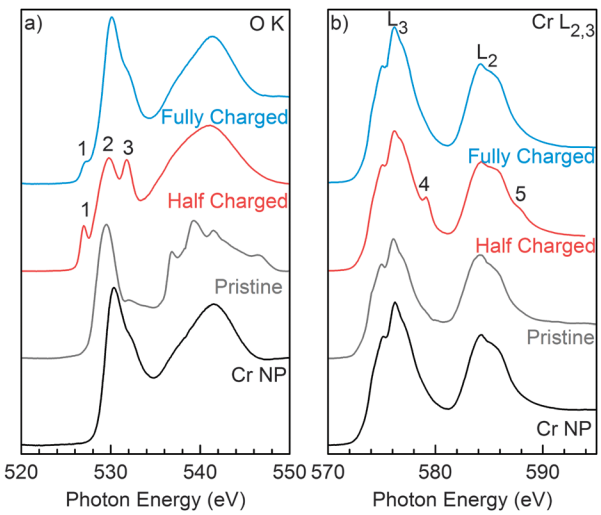

Fig. 7 XAS TEY spectra recorded at the O K and Cr $L_{2,3}$ edges for as-purchased Cr NP, pristine, half-charged, and fully charged carbon-free Cr:Li_2O_2 electrodes. Electrochemical data for the half-charged and fully-charged Cr:Li_2O_2 electrodes are shown in Fig. 6. Energies are calibrated to the Cr L_2-edge positions. Processing of spectral intensities is described in the experimental section.

This journal is © the Owner Societies 2014

Published on 29 novembr 2013. Downloaded by University of Chicago on 2020.04.13. 2:21:20.

literature,[38–40] indicating pronounced oxidation on the surface of Cr NP.

Pristine Cr:Li_2O_2 electrodes showed the expected features of both Cr NP and Li_2O_2 (Fig. 7). After partially charging the electrodes, new peaks labeled (1), (2) and (3) in the O K-edge (Fig. 7a) and (4) and (5) in the Cr $L_{2,3}$-edges (Fig. 7b) appeared. Using the reference spectra of Li_2CO_3,[16] Li_2O_2,[16,41] and LiO_2 (ref. 42) after appropriate shifts to a common energy scale (Fig. S13, ESI†), peak (1) can be attributed to the ligand hole in the O p band associated with Cr^{6+} (ref. 43) or the π^* resonance of superoxide $(O{=}O)^-$ bonds such as in LiO_2,[42,44] which may have formed on Li_2O_2 oxidation.[13] This presence of Cr^{6+} is further supported by the presence of peaks (4) and (5) in the Cr L_3 and L_2 edges, which is characteristic of Cr^{6+} (ref. 45). Peak (2) results from the convolution of pre-edge features of Li_2O_2 and the ligand hole in the O p band associated with Cr^{3+} such as Cr_2O_3 appearing around 530 eV, and (3) can be assigned to Li_2CO_3 formed from electrolyte decomposition during charging. Upon complete charging of the Cr:Li_2O_2 electrode, peaks (2)–(5) disappeared but peak (1) remained (Fig. S14, ESI†). The XAS evidence of Cr^{3+} oxidation to Cr^{6+} and possible formation of LiO_2 support the previous hypothesis that the kinetics of Li_2O_2 oxidation can be enhanced by the rate-limiting step in the first delithiation step ($Li_2O_2 \rightarrow LiO_2 + Li^+ + e^-$).[46] The ability of Cr NP to accommodate mixed valence states on the surfaces can facilitate electron removal from Li_2O_2 through the redox of $Cr^{3+} \leftrightarrow Cr^{6+}$ during the first-electron oxidation step, promoting the Li_2O_2 oxidation kinetics.

Conclusions

Here we report no clear trend in the activities of perovskite oxides against Li_2O_2 oxidation ($LaCrO_3 \gg$ BSCF > $LaNiO_3 \approx LaMnO_{3+\delta} \approx LaFeO_3$) *versus* their e_g-filling, in contrast to oxygen electrocatalysis in alkaline solution reported previously.[30,31] This finding strongly points to a different catalytic pathway for Li_2O_2 oxidation compared to H_2O oxidation. Cr-based catalysts such as $LaCrO_3$, Cr_2O_3 and Cr NP with oxidized surfaces, which have negligible activity for aqueous OER, have shown surface-area-specific oxidation activities that rival those of highly active noble metal catalysts such as Pt/C and Ru/C but without promoting electrolyte oxidation. The mass-specific activity of Cr NP is ~50 times higher than VC, and remained active for Li_2O_2 oxidation at 3.8 V_{Li}. Such facile kinetics for Li_2O_2 oxidation is confirmed in Li–O_2 cells, where a significant ~400 mV reduction in the charging voltage is achieved in the presence of 40-nm Cr NP mechanically mixed with VC. It is proposed that the ability of Cr compounds to accommodate mixed valence states of Cr^{3+} and Cr^{6+} ions on the surfaces can promote Li_2O_2 oxidation kinetics by facilitating electron removal necessary to carry out the first-electron oxidation step of Li_2O_2 to LiO_2. XAS data for pristine, partially charged, and fully charged electrodes support this hypothesis by revealing the redox of $Cr^{3+} \leftrightarrow Cr^{6+}$ during Li_2O_2 oxidation and possible formation of oxygen species akin to LiO_2 superoxide.

Acknowledgements

This work was supported by Toyota Motor Europe. Canadian Light Source is supported by the NSERC, NRC, CIHR of Canada, the Province of Saskatchewan, WEDC and the University of Saskatchewan. The authors acknowledge the valuable inputs of Jonathon Harding in gathering and processing the XPS data presented herein.

Notes and references

1 P. G. Bruce, S. A. Freunberger, L. J. Hardwick and J. M. Tarascon, *Nat. Mater.*, 2012, **11**, 19–29.
2 Y.-C. Lu, H. A. Gasteiger, M. C. Parent, V. Chiloyan and Y. Shao-Horn, *Electrochem. Solid-State Lett.*, 2010, **13**, A69–A72.
3 Y.-C. Lu, D. G. Kwabi, K. P. C. Yao, J. R. Harding, J. Zhou, L. Zuin and Y. Shao-Horn, *Energy Environ. Sci.*, 2011, **4**, 2999–3007.
4 K. U. Schwenke, S. Meini, X. Wu, H. A. Gasteiger and M. Piana, *Phys. Chem. Chem. Phys.*, 2013, **15**, 11830–11839.
5 V. S. Bryantsev, V. Giordani, W. Walker, M. Blanco, S. Zecevic, K. Sasaki, J. Uddin, D. Addison and G. V. Chase, *J. Phys. Chem. A*, 2011, **115**, 12399–12409.
6 R. Black, S. H. Oh, J. H. Lee, T. Yim, B. Adams and L. F. Nazar, *J. Am. Chem. Soc.*, 2012, **134**, 2902–2905.
7 S. A. Freunberger, Y. Chen, N. E. Drewett, L. J. Hardwick, F. Bardé and P. G. Bruce, *Angew. Chem., Int. Ed.*, 2011, **50**, 8609–8613.
8 V. S. Bryantsev and F. Faglioni, *J. Phys. Chem. A*, 2012, **116**, 7128–7138.
9 D. Sharon, V. Etacheri, A. Garsuch, M. Afri, A. A. Frimer and D. Aurbach, *J. Phys. Chem. Lett.*, 2012, **4**, 127–131.
10 B. M. Gallant, R. R. Mitchell, D. G. Kwabi, J. Zhou, L. Zuin, C. V. Thompson and Y. Shao-Horn, *J. Phys. Chem. C*, 2012, **116**, 20800–20805.
11 J. S. Hummelshøj, A. C. Luntz and J. K. Norskøv, *J. Chem. Phys.*, 2013, **138**, 034703–034712.
12 Y.-C. Lu, B. M. Gallant, D. G. Kwabi, J. R. Harding, R. R. Mitchell, M. S. Whittingham and Y. Shao-Horn, *Energy Environ. Sci.*, 2013, **6**, 750–768.
13 Y.-C. Lu and Y. Shao-Horn, *J. Phys. Chem. Lett.*, 2013, **4**, 93–99.
14 V. Viswanathan, K. S. Thygesen, J. S. Hummelshøj, J. K. Norskøv, G. Girishkumar, B. D. McCloskey and A. C. Luntz, *J. Chem. Phys.*, 2011, **135**, 214704.
15 B. D. McCloskey, R. Scheffler, A. Speidel, D. S. Bethune, R. M. Shelby and A. C. Luntz, *J. Am. Chem. Soc.*, 2011, **133**, 18038–18041.
16 B. M. Gallant, D. G. Kwabi, R. R. Mitchell, J. Zhou, C. V. Thompson and Y. Shao-Horn, *Energy Environ. Sci.*, 2013, **6**, 2518.
17 S. H. Oh and L. F. Nazar, *Adv. Energy Mater.*, 2012, **2**, 903–910.
18 J.-H. Lee, R. Black, G. Popov, E. Pomerantseva, F. Nan, G. A. Botton and L. F. Nazar, *Energy Environ. Sci.*, 2012, **5**, 9558–9565.

Published on 29 novembr 2013. Downloaded by University of Chicago on 2020.04.13. 2:21:20.

19 R. R. Mitchell, B. M. Gallant, C. V. Thompson and Y. Shao-Horn, *Energy Environ. Sci.*, 2011, **4**, 2952–2958.
20 Y. Chen, S. A. Freunberger, Z. Peng, F. Bardé and P. G. Bruce, *J. Am. Chem. Soc.*, 2012, **134**, 7952–7957.
21 Z. Peng, S. A. Freunberger, Y. Chen and P. G. Bruce, *Science*, 2012, **337**, 563–566.
22 L. Brandsma, J. Meijer and H. D. Verkruijsse, *Recl. Trav. Chim. Pays-Bas*, 1976, **95**, 79–80.
23 G. V. Chase, S. Zecevic, T. W. Wesley, J. Uddin, K. A. Sasaki, P. G. Vincent, V. Bryantsev, M. Blanco and D. D. Addison, *U S Pat.*, US20120028137 A1, 2012.
24 Y. Chen, S. A. Freunberger, Z. Peng, O. Fontaine and P. G. Bruce, *Nat. Chem.*, 2013, **5**, 489–494.
25 J. R. Harding, Y. C. Lu, Y. Tsukada and Y. Shao-Horn, *Phys. Chem. Chem. Phys.*, 2012, **14**, 10540–10546.
26 Y. Yang, M. Shi, Y.-S. Li and Z.-W. Fu, *J. Electrochem. Soc.*, 2012, **159**, A1917–A1921.
27 V. Giordani, S. A. Freunberger, P. G. Bruce, J. M. Tarascon and D. Larcher, *Electrochem. Solid-State Lett.*, 2010, **13**, A180–A183.
28 K.-N. Jung, J.-I. Lee, W. B. Im, S. Yoon, K.-H. Shin and J.-W. Lee, *Chem. Commun.*, 2012, **48**, 9406–9408.
29 S. H. Oh, R. Black, E. Pomerantseva, J.-H. Lee and L. F. Nazar, *Nat. Chem.*, 2012, **4**, 1004–1010.
30 J. Suntivich, H. A. Gasteiger, N. Yabuuchi, H. Nakanishi, J. B. Goodenough and Y. Shao-Horn, *Nat. Chem.*, 2011, **3**, 546–550.
31 J. Suntivich, K. J. May, H. A. Gasteiger, J. B. Goodenough and Y. Shao-Horn, *Science*, 2011, **334**, 1383–1385.
32 J. Suntivich, H. A. Gasteiger, N. Yabuuchi and Y. Shao-Horn, *J. Electrochem. Soc.*, 2010, **157**, B1263–B1268.
33 Y.-C. Lu, H. A. Gasteiger and Y. Shao-Horn, *J. Am. Chem. Soc.*, 2011, **133**, 19048–19051.
34 T. Regier, J. Krochak, T. K. Sham, Y. F. Hu, J. Thompson and R. I. R. Blyth, *Nucl. Instrum. Methods Phys. Res., Sect. A*, 2007, **582**, 93–95.
35 R. Black, J. H. Lee, B. Adams, C. A. Mims and L. F. Nazar, *Angew. Chem., Int. Ed.*, 2013, **52**, 392–396.
36 M. García-Mota, M. Bajdich, V. Viswanathan, A. Vojvodic, A. T. Bell and J. K. Nørskov, *J. Phys. Chem. C*, 2012, **116**, 21077–21082.
37 S. Kang, Y. Mo, S. P. Ong and G. Ceder, *Chem. Mater.*, 2013, **25**, 3328–3336, DOI: 10.1021/cm401720n.
38 T. Schedel-Niedrig, *Fresenius' J. Anal. Chem.*, 1998, **361**, 680–682.
39 M. O. Figueiredo, A. C. dos Santos, M. J. Carmezim, M. Abbate, F. M. F. de Groot, H. Petersen and W. Braun, *Analyst*, 1994, **119**, 609–611.
40 F. M. F. de Groot, M. Grioni, J. C. Fuggle, J. Ghijsen, G. A. Sawatzky and H. Petersen, *Phys. Rev. B: Condens. Matter Mater. Phys.*, 1989, **40**, 5715–5723.
41 R. Qiao, Y.-D. Chuang, S. Yan and W. Yang, *PLoS One*, 2012, **7**, e49182.
42 M. W. Ruckman, J. Chen, S. L. Qiu, P. Kuiper, M. Strongin and B. I. Dunlap, *Phys. Rev. Lett.*, 1991, **67**, 2533–2536.
43 D. W. Fischer, *J. Phys. Chem. Solids*, 1971, **32**, 2455–2480.
44 J. Stöhr, *NEXAFS Spectroscopy*, Springer, Berlin, 2003.
45 T. L. Daulton and B. J. Little, *Ultramicroscopy*, 2006, **106**, 561–573.
46 L. Zhong, R. R. Mitchell, Y. Liu, B. M. Gallant, C. V. Thompson, J. Y. Huang, S. X. Mao and Y. Shao-Horn, *Nano Lett.*, 2013, **13**, 2209–2214.

 This journal is © the Owner Societies 2014